NUMERICAL SIMULATION OF LOW REYNOLDS NUMBER TURBULENT FLOW IN A RECTANGULAR ANNULAR DUCT

H. Xu and **M. Khalid**
Institute for Aerospace Research, National Research Council,
Ottawa, Ontario, K1A 0R6, CANADA

A. Pollard
Department of Mechanical Engineering, Queen's University,
Kingston, Ontario, K7L 3N6, CANADA

ABSTRACT

The paper investigates low Reynolds number turbulent flow in a rectangular annular duct with side-wall aspect ratios of 4:2 for the outer duct and 2:1 for the inner duct. The Reynolds number was 150 based on the width of the inner rectangular duct, w, and the mean frictional velocity, u_τ. Large Eddy Simulations (LES) were performed with grid sizes of $128\times66\times66$ and $128\times130\times66$ using the Smagorinsky Subgrid Scale (SGS) model. Then, a Direct Numerical Simulation (DNS) with a grid resolution of $128\times258\times130$ was performed using the refined LES solution as the initial conditions.

The flow on the minor side of the channel was turbulent-like, with the streamwise velocity exhibiting typical turbulent viscous and logarithmic regions. On the major side, the flow appeared laminar-like with the streamwise velocity along wall-bisector exhibiting a Poiseuille laminar profile. The mean turbulence-driven secondary flow appeared as a chain of counter-rotating vortical flows in the near-wall and near-corner regions. The highly anisotropic and coherent Reynolds stress distributions were obtained and analyses of these Reynolds stresses revealed the generation mechanisms of the turbulence-driven secondary flow. The one-dimensional energy spectra suggested strong anisotropy in the small-scale motions near the convex corners.

INTRODUCTION

The turbulent flow in the vicinity of a streamwise corner is of engineering interest, with relevance to a complex three-dimensional turbulent flow that has two inhomogeneous directions. Prandtl [1926] first studied the origins of the flow perpendicular to the streamwise direction in a generic duct. As outlined by Bradshaw [1987], two distinct mechanisms were found responsible for generating the secondary flows: the skew-induced vortex generation by quasi-inviscid deflection of existing mean vorticity, and the stress-induced vortex generation by anisotropy and inhomogeneous Reynolds stresses. Theoretical analyses and experimental measurements in rectangular ducts with various aspect ratios can be found in, for example, Nikuradse [1930], Gessner & Jones [1965], Perkins [1970] and Gerard [1978]. Demuren & Rodi [1984] reviewed the experimental work and Reynolds-averaged Navier-Stokes (RANS) turbulence models that focus on the turbulence-driven secondary flows in both square and rectangular ducts.

A number of numerical simulations for turbulent flows in a square duct have been reported. Prior to DNS and LES, RANS approaches were used. As expected, closure models based on the assumptions of isotropy fail to predict any turbulence-driven secondary flow. The anisotropy of the Reynolds stresses in turbulence closure models was addressed by Launder & Ying [1973], Speziale [1987] and Naimi & Gessner [1997] for flows in both square and rectangular ducts. Gavrilakis [1992] performed a DNS at a Reynolds number of 4410, and found reasonable agreement with experimental data of the mean flow and turbulence statistics from Niederschulte [1989] and Nishino & Kasagi [1989]. The fully developed turbulent flow in a square duct at a higher Reynolds number of 10,320 was investigated by Huser & Biringen [1993] using a spectral/high-order finite-difference scheme and a time-splitting integration method. Quadrant analysis was used to explain the mechanisms for generating the off-diagonal Reynolds stresses. By connecting specific turbulence structures to the generation of the anisotropic Reynolds stresses, further physical understanding was provided about the generation of secondary flow. LES was used to study the flow in a square duct by Madabhushi & Vanka [1991], Breuer & Rodi [1994], Kajishima & Miyake [1992] and Xu [1997]. Xu & Pollard [2001] considered a turbulent flow in square (1:1 aspect ratio) annular ducts, which featured both concave and convex 90° corners. Comparison between the LES of a square annular duct flow and the DNS of a square duct flow clearly indicated that the major anisotropy of the Reynolds stresses near both concave and convex 90° corners was accurately captured and, therefore, the turbulence-driven secondary flow was correctly predicted. Xu, Khalid & Pollard [2002] investigated a rectangular duct flow with a 2:1 aspect ratio; this study was aimed at systematically

investigating the dependence of the Reynolds stress anisotropy on the aspect ratios of rectangular ducts.

In the current paper, we extend the earlier work from a square annular duct to the rectangular annular duct with side-wall aspect ratios of 4:2 for the outer duct and 2:1 for the inner duct, as shown in Fig. 1. To the best of our knowledge, there are no previous LES or DNS investigations of a flow in such a configuration. The physical problem is more complicated here since the convex and concave corners in the rectangular annular duct are not aligned with each other along their corner bisector lines. This misalignment creates increased anisotropy in the Reynolds stress distributions and hence more complicated turbulence-driven secondary flow.

LES with a $128\times66\times66$ grid was performed using the conventional Smagorinsky Subgrid Scale (SGS) model. These "data" were used as the initial conditions to conduct a refined LES with a $128\times130\times66$ grid. The refined LES results were then used as the initial conditions for a DNS using a $128\times258\times130$ grid in the x, y, z directions, respectively. The Reynolds number was 150 based on the width of the inner rectangular duct, w, in Fig. 1, and the mean frictional velocity, u_τ. The time-averaged one-dimensional energy spectra were obtained at a number of sampling points in the rectangular annular duct.

The one important aspect of this research will be a detailed investigation of the Reynolds stress-induced secondary flow near the tip as the aspect ratio (L/w) of the inner rectangular duct in Fig. 1 approaches infinity. As stated by Piquet [1999], "the capture of the correct intensity of the stress-driven tip vortex (and of its induced influence of the wall pressure distribution) is a difficult turbulence problem." The present paper is an initial effort toward solving the problem of the stress-driven tip vortex, which can be accomplished by investigating a number of aspect ratios (L/w) of the inner rectangular duct.

NUMERICAL METHODS

The governing equations are the unsteady incompressible Navier-Stokes (N-S) equations. In the current LES investigation, the Smagorinsky SGS model was used and a wall damping function, Kajishima & Miyake [1992], was applied.

The initial conditions for the preliminary LES of the flow inside the rectangular annular ducts were generated from the fully-developed laminar velocity flow upon which was superimposed disturbances that were solutions to the Orr-Sommerfeld (O-S) equation, as described in Xu & Pollard [2001].

The DNS study was conducted using the interpolated LES results as the initial conditions. The SGS model and wall damping function were switched off in the DNS investigation and the unsteady incompressible N-S equations are completely solved.

The governing equations were spatially discretized using a second-order finite volume method on a staggered grid. As demonstrated by Kim & Moin [1985], a common practice for the temporal discretization of the N-S equations is to apply the second-order Adams-Bashforth scheme for the convection terms and the second-order Adams-Moulton scheme for the diffusion terms. The explicit treatment of the non-linear terms eliminates the need to linearize the set of equations and the implicit treatment of the diffusion terms enhances the numerical stability. The fractional step method in Kim & Moin [1985] was used to de-couple the pressure and the velocity and to obtain the time-dependent pressure and the divergence-free velocity.

The non-dimensional grid spacing in the streamwise direction had a uniform distribution of $\Delta x^+ = 14.73$, which was sufficient to resolve the complete energy spectrum in the streamwise direction, as shown in turbulent kinetic energy spectrum analysis provided below.

The computations were conducted at three grid resolutions in the cross-streamwise direction:

1. LES with a grid of $N_x\times N_y\times N_z = 128\times66\times66$ so that $\Delta y^+_{max} = 17.842$, $\Delta z^+_{max} = 8.921$ and $\Delta y^+_{min} = 2.058$, $\Delta z^+_{min} = 1.029$;
2. LES with a grid of $N_x\times N_y\times N_z = 128\times130\times66$ so that $\Delta y^+_{max} = \Delta z^+_{max} = 8.921$ and $\Delta y^+_{min} = \Delta z^+_{min} = 1.375$;
3. DNS with a grid of $N_x\times N_y\times N_z = 128\times258\times130$ so that $\Delta y^+_{max} = \Delta z^+_{max} = 4.764$ and $\Delta y^+_{min} = \Delta z^+_{min} = 0.4407$.

The quality of the solution was guaranteed by driving the residuals of both the continuity and momentum equations at each time step down to the computer machine error. A grid dependence study confirmed that a grid of $N_x\times N_y\times N_z = 128\times258\times130$ was sufficient to resolve the flow in the non-homogeneous cross-streamwise direction.

PRESENTATION and DISCUSSION OF RESULTS

The non-dimensional computational domain, as shown in Fig. 1, was located between the outer rectangular duct, with a size of $4\pi\times4\times2$, and the inner rectangular duct, with a size of $4\pi\times2\times1$. A computational time step of $\Delta t = 2.5\times10^{-4}$, non-dimensionalized by the large eddy turnover time ($LETOT = w/u_\tau$), was used for both DNS and LES, which guaranteed the CFL number below 0.5. Comparisons of the DNS and LES results indicated that the grid dependence effects are minor in the cross-streamwise direction. This grid dependence study and the turbulence energy spectrum analysis suggest that a grid resolution of

$N_x \times N_y \times N_z = 128 \times 258 \times 130$ is sufficient to produce reliable DNS results at the current Reynolds number.

The one-dimensional turbulence energy spectra are plotted in Fig. 2 (a), (b), (c) at three typical points on the cross-streamwise plane. The coordinates of these three points are:
(a) $(y,z) = (0.011, 0.0128)$, near the concave corner bisector of the outer rectangular duct;
(b) $(y,z) = (0.4699, 0.4964)$, in the core of the flow;
(c) $(y,z) = (0.9805, 0.4964)$, near the convex corner of the inner rectangular duct.
The spectra are presented in their "raw" form, but we have used the mean frictional velocity as a scaling factor in the N-S equations.

As shown in Fig. 2(a), the streamwise velocity energy content far exceeds the spanwise components in the concave corner region. This is consistent with spectra obtained by Huser and Biringen [1993]. Also, the –5/3 region is rather narrow, which is expected for low Reynolds number flow. Based on these spectra, the LES results should be viewed with some suspicion as to the adequacy of the SGS model.

Fig. 2(b) presents the spectrum in the "core" of the flow, far away from the corner and wall regions. This region more-or-less mimics the core region of the flow in a square duct. The spectra are more isotropic, but retain differences at the lower wave numbers. The turbulent flow quickly approaches to the isotropic state in the small-scale regime.

Fig. 2(c) shows the turbulence energy spectrum near the convex corner of the inner rectangular duct. Since the damping effects of a convex corner are not as strong as a concave corner, (see Xu & Pollard [2001]), the anisotropy of the turbulence motion is visible but not as pronounced as that near the concave corner region. However, the high wave number region shows pronounced "tails" that might suggest incomplete resolution.

The mean streamwise velocity contours and the turbulence-driven secondary flow are shown in Figs. 3 and 4, respectively. As expected, the bulge in the streamwise velocity contours follows the direction of the turbulence-driven secondary flow. For example, the contours in Fig. 3 bulge towards the inner wall along the wall bisector on the minor side. Correspondingly, Fig. 4, colored by the secondary velocity magnitude, indicates a flow toward the inner wall along the wall bisector on the minor side. Similar observations can be made near the convex corner regions.

The streamwise velocity profiles are plotted along the wall bisector and the line passing through the convex corner on both the major and minor sides of the rectangular annular duct, in Figs. 5 and 6(a), (b), respectively. The LES and DNS results are within a few percent of each other, which suggests that the discrepancies in the spectra, while important, have little effect on the mean, as expected. We continue to investigate the validity of both simulation results.

DNS results along the wall bisector and the convex corner for both inner and outer walls are presented in Fig. 7. The mean streamwise velocity in Fig. 7 is normalized by the mean friction velocity, u_τ, the definition of which can be found in Xu & Pollard [2001].

As stated by Gavrilakis [1992], the variation of local mean wall shear stress, and therefore the local friction velocity, over the duct boundaries introduces an ambiguity as to which scale should be used. Within the viscous sublayer, the local friction velocity ought to be the correct choice. Fig. 8 shows the variation of wall stress ratio along both the inner and outer walls on the minor side. The u^+ distributions in Fig. 7 can then be corrected by the local friction velocities based on the data in Fig. 8. Fig. 9, therefore, shows the corrected near-wall behavior of u^+. The corrected u^+ deviates from the standard logarithmic relation rather sharply near the convex corner region. The shape of the $u^+ \sim y^+$ curve for this region is reminiscent of that found in a manipulated boundary layer flow, Pollard [1997].

Thus, we speculate that both laminar-like and turbulent flow coexist at the current Reynolds number in the rectangular annular duct. The flow in the channel on the minor side is turbulent and the near-wall behavior exhibits the typical turbulent viscous-layer and logarithmic distributions. The flow in the channel on the major side is laminar since the streamwise velocity along the wall bisector takes the form of the Poiseuille laminar profile, see Figure 5. This observation is further confirmed by an instantaneous visualization of turbulent structures using the technique proposed by Hunt et al. [1998], as shown in Fig. 10(a). Most of the turbulent fluctuation occurs in the flow channel on the minor side while the flow channel on the major side is pretty quiet. An instantaneous flow field visualization in the perspective view in Fig. 10(b) reveals the spiraling structures near the convex corners of the inner rectangular duct.

The mean turbulence-driven secondary flow presents a chain of counter-rotating vortical flows in the near-wall and near corner regions. In reference to Figure 4, there exists a counter-rotating vortex pair, a very strong vortex on the convex corner of the major side and a weaker vortex on the minor side of the inner rectangular duct. We anticipate that, with reference to earlier results from a square annular duct, (Xu & Pollard [2001]), as the aspect ratio increases, say from 4:2/2:1 to 6:3/3:1.5, the vortex on the major side will become more pronounced and dominant, while the minor-side vortex will become weaker near the convex corner. It is reasonable to foresee that these vortices are the embryonic form of stress-induced tip vortices.

Figs. 11 (a), (b) and (c) present the spanwise distributions of the spatial and temporal-averaged Reynolds stresses ($u'u'$, $u'v'$ and $v'w'$). We note that, when compared to the distributions found in a square annular duct (Xu & Pollard [2001]), the change in the aspect ratio causes significant alterations to the distributions of the highly anisotropic

Reynolds stress. An analysis of these Reynolds stresses reveals the mechanisms for the generation of the turbulence-driven secondary flow. Space precludes detailed presentation of these results; they will be presented at the Symposium.

CONCLUSIONS

DNS and LES have been performed for low Reynolds number turbulent flows in a rectangular annular duct with side-wall aspect ratios of 4:2 for the outer duct and 2:1 for the inner duct at a Reynolds number $\mathrm{Re}_\tau = 150$. The following conclusions can be drawn:

(1) Based upon both mean and $u^+ \sim y^+$ velocity plots, laminar-like and turbulent flows coexist in the rectangular annular duct.
(2) The time-averaged turbulent energy spectra reveal the presence of strong anisotropy. The magnitude of the anisotropy is region-dependent.
(3) The mean turbulence-driven secondary flow consists of a chain of counter-rotating vortical flows in the near-wall and near corner regions. The intensity of the vortical motions is non-symmetric around the convex corners of the inner duct.

ACKNOWLEDGEMENTS

The authors would like to acknowledge the assistance of Ms. D. VanWeelden, Queen's University, for preparing flow visualization figures. Andrew Pollard acknowledges the financial support of NSERC.

REFERENCES

P. Bradshaw, Ann. Rev. Fluid Mech., Vol. 19, 1987.
M. Breuer and W. Rodi, ERCOFTAC Bulletin, 22, 1994.
A.O. Dumuren and W. Rodi, J. Fluid Mech., 140, 1984.
S. Gavrilakis, J. Fluid Mech., Vol. 244, 1992.
R. Gerard, J. of Hydraulics Division, HY5, May 1978.
F.B. Gessner and J.B. Jones, J. Fluid Mech., 23, 4, 1965.
J.C.R. Hunt, A. A. Wray and P. Moin, Center for Turbulence Research, CTR-S88, 1998.
A. Huser and S. Biringen, J. Fluid Mech., 257, 1993.
T. Kajishima and Y. Miyake, Computers Fluids, 21, 1992.
J. Kim and P. Moin, J. of Computational Physics, 59, 1985
B.E. Launder and W.M. Ying, Proc. Inst. Mech. Eng., 187, 455, 1973.
R.K. Madabhushi and S.P. Vanka, Phys. Fluids A 3(11), 1991.
M. Naimi and F.B. Gessner, Trans. of the ASME, J. Fluid Eng., 119, 1997.
M.A. Niederschulte, Ph.D thesis, University of Illinois at Urbana-Champaign, 1989.
J. Nikuradse, Turbulente Strömung in nicht-kreisformigen Röhren, Ing. Arch. 1, 1930.
K. Nishino and N. Kasagi, 7th Symp. on Turbulent Shear Flows, Stanford University, 1989.
H. J. Perkins, J. Fluid Mech., 44, 1970.
J. Piquet, Turbulent Flows-Models and Physics, Springer-Verlag 1999.
A. Pollard, Progress in Aerospace Sciences, 33, 1997.
L. Prandtl, 2nd Intl. Köng. Für Tech. Mech., Zürich, 1926 [NACA Tech. Memo. 435, 62].
C.G. Spiezale, J. Fluid Mech., Vol. 178, 1987.
H. Xu, Ph.D. Thesis, Department Mechanical Engineering, Queen's University, 1997.
H. Xu and A. Pollard, Phys. of Fluids, 13(11), 2001.
H. Xu, M. Khalid and A. Pollard, 9th European Turbulence Conference, Southampton, U.K. May 2002.

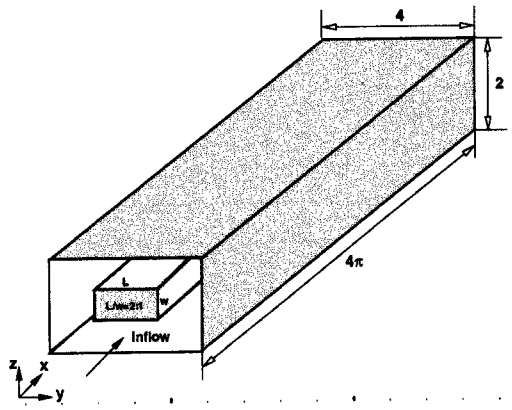

Fig. 1: Rectangular Annular Duct Geometry

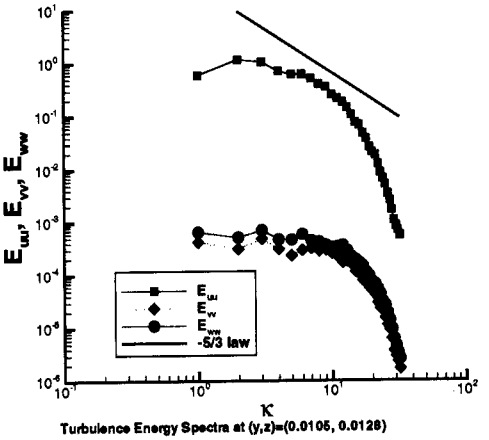

(a)

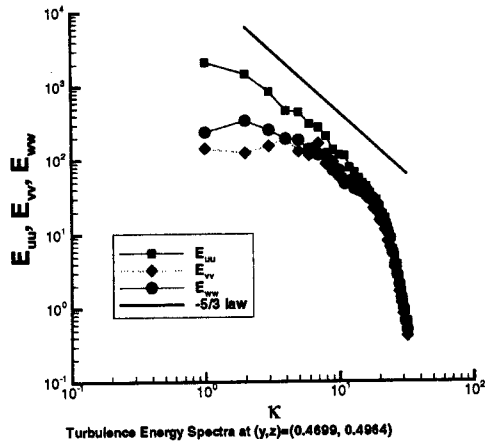

(b)

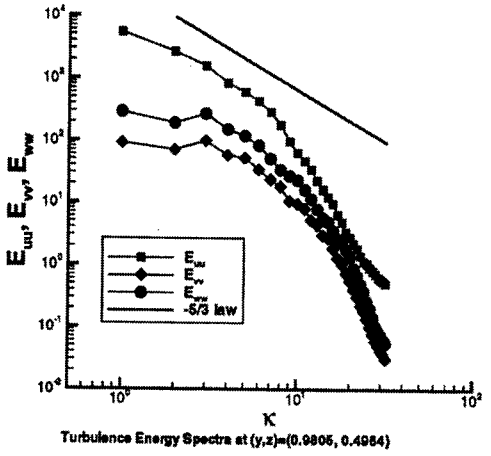

(c)

Fig. 2: Mean turbulence energy spectra

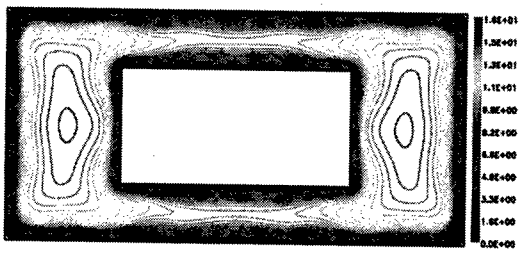

Fig.3: Mean streamwise velocity contours

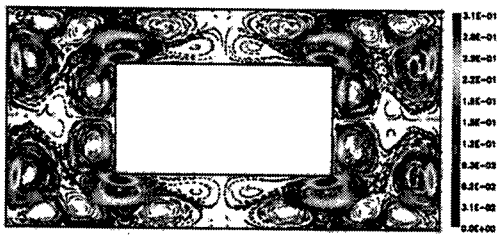

Fig. 4: Mean turbulence-driven secondary flow.

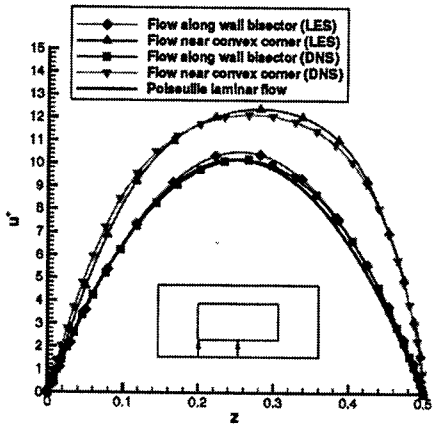

Fig. 5: Mean streamwise velocity profiles in the minor axis direction

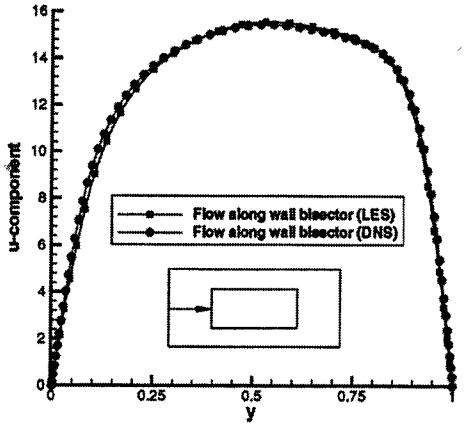

(a)

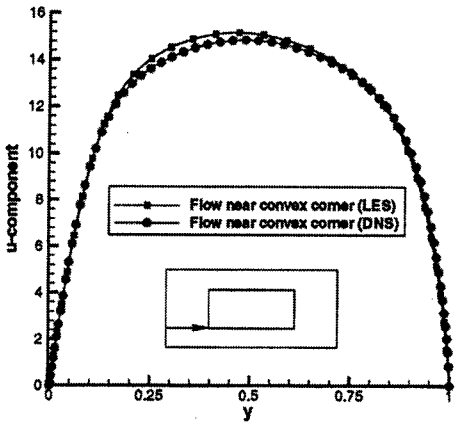

(b)

Fig. 6: Mean streamwise velocity profiles in the major axis direction

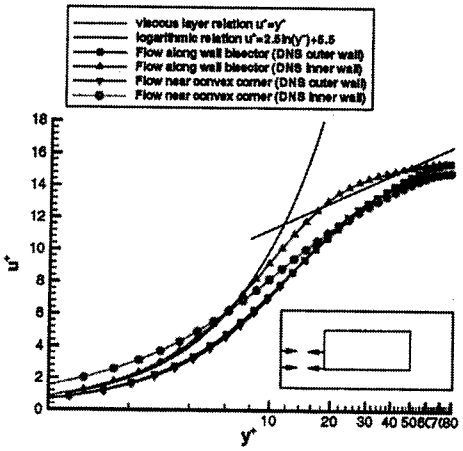

Fig. 7: Near-wall behavior of streamwise velocity normalized using mean friction velocity

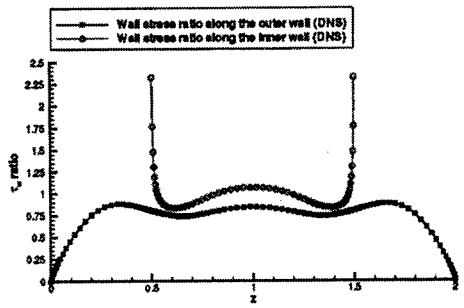

Fig. 8: Wall stress ratio along both inner and outer side walls on the minor side of the rectangular annular duct

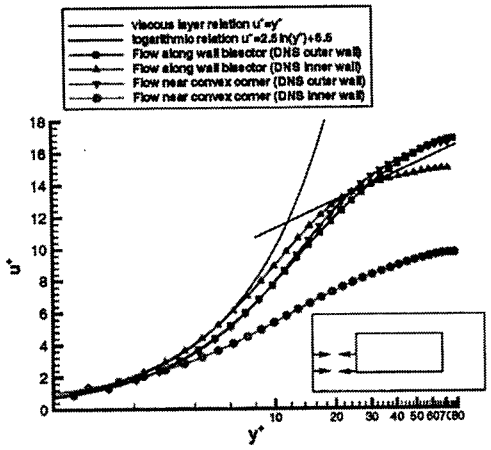

Fig. 9: Near-wall behavior of streamwise velocity normalized by the local friction velocity

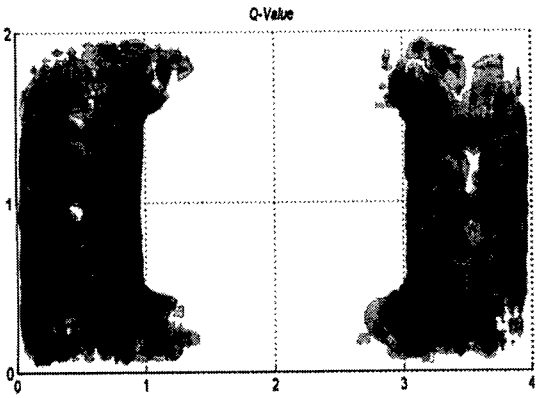

(a) cross-section view X/h~20

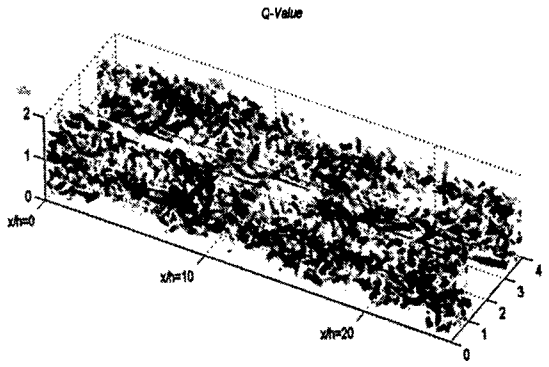

(b) perspective view

Fig. 10: Instantaneous flow visualization using the technique proposed by Hunt et al. [1998]

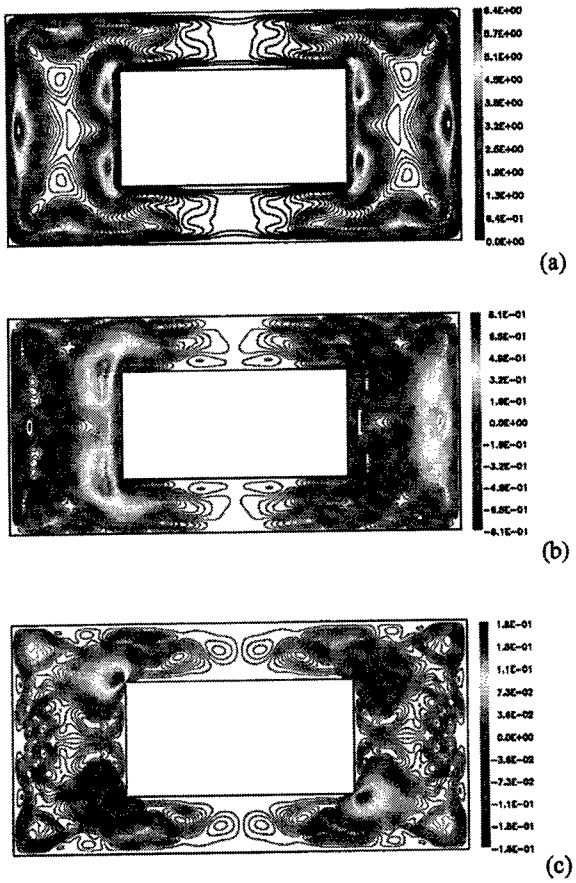

Fig. 11: Reynolds stress distributions in the rectangular annular duct: (a) $u'u'$, (b) $u'v'$ and (c) $v'w'$